9

Energetic particle radiation

9.1 Definitions

Terminology relating to details of the environment is defined in detail in later sub-sections and in Annex G (e.g. solar particle events, radiation belts). Only the main common terms are described here.

9.1.1 Energetic particle

In the context of space systems radiation effects, energetic particles are particles which can penetrate outer surfaces of spacecraft. For electrons, this is typically above 100keV, while for protons and other ions this is above 1MeV. Neutrons, gamma-rays and X-rays are also considered energetic particles in this context.

9.1.2 Radiation

The transfer of energy by means of a particle (including photons). In the context of this chapter, electromagnetic radiation below the X-ray band is excluded. This therefore excludes UV, visible, thermal, microwave and radio-wave radiation.

9.1.3 Dose, absorbed dose, dose equivalent

Dose is a quantity of radiation delivered at a position. In its broadest sense it can include the flux of particles, but in the context of space energetic particle radiation effects, it usually refers to the energy absorbed locally per unit mass as a result of radiation exposure. This energy may be transferred through ionization and excitation, in which case it is often referred to as absorbed dose. Dose equivalent refers to a quantity normally applied to biological effects and includes scaling factors to account for the more severe effects of certain kinds of radiation. A portion of the energy absorption can result in damage to the lattice structure of solids through displacement of atoms, and this is now commonly referred to as Non-Ionizing Energy Loss (NIEL).

9.1.4 Flux

The amount of radiation crossing a surface per unit of time, often expressed in “integral form” as particles per unit area per unit time (e.g. electrons.cm^{-2}.s^{-1}) above a certain threshold energy. The directional flux is differential with respect to solid angle (e.g. particles.cm^{-2}.steradian^{-1}.s^{-1}) while the “differential” flux is differential with respect to energy (e.g. particles. cm^{-2}.MeV^{-1}.s^{-1}). In some cases fluxes are also treated as differential with respect to Linear Energy Transfer (see below).

9.1.5 Fluence

A time-integration of the flux.

9.1.6 Current

The term current is often used in discussion of radiation transport to refer to the rate of transport of particles through a boundary. In contrast to flux, current is dependent on the direction in which the particle crosses the boundary (it is a vector integral). An isotropic omnidirectional flux, f, incident on a plane gives rise to a current of ¼.f normally in each direction across the plane.

9.1.7 Isotropic

A property of a distribution of particles where the flux is constant over all directions.

9.1.8 Omnidirectional

An omnidirectional flux is defined as the scalar integral of the flux over all directions. This implies that no consideration is taken of the directional distribution of the particles which can be non-isotropic. The flux at a point is the number of particles crossing a sphere of unit cross-sectional surface area (i.e. of radius $1/\sqrt{\pi}$). An omnidirectional flux should not be confused with an isotropic flux.

9.1.9 Equivalent fluence

A quantity which attempts to represent the damage at different energies and from different species. Damage coefficients are used to scale the effect caused by particles to the damage caused by a standard particle and energy. For example, for solar cell degradation it is often taken that one 10MeV proton is “equivalent” to 3000 1MeV electrons. This concept also occurs in consideration of non-ionizing energy loss effects (NIEL).

9.1.10 LET

Linear Energy Transfer. The rate of energy deposit from a slowing energetic particle with distance travelled in matter, the energy being imparted to the material. Normally used to describe the ionization track caused by passage of an ion. LET is material-dependent and is also a function of particle energy. For ions of concern in space radiation effects, it increases with decreasing energy (it also increases at high energies, beyond the *minimum ionizing* energy). LET allows different ions to be considered together by simply representing the ion environment as the summation of the fluxes of all ions as functions of their LETs. This simplifies single-event upset calculation. The rate of energy loss of a particle, which also includes emitted secondary radiations, is the *stopping power*.

9.1.11 Solar flare

An emission of optical, UV and X-radiation from an energetic event on the sun. There is some controversy about the causal relationship between solar flares and the arrival of large fluxes of energetic particles at Earth. Therefore, it is more consistent to refer to the latter as solar energetic particle events (SEPEs). There is a strong link between the injection and acceleration of energetic electrons following the impingement of a solar coronal mass ejection (CME) on the earth’s magnetosphere.

9.1.12 Bremsstrahlung

High-energy electromagnetic radiation in the X-γ energy range emitted by charged particles slowing down by scattering off atomic nuclei. The primary particle might ultimately be absorbed while the bremsstrahlung can be highly penetrating. In space, the most common source of bremsstrahlung is electron scattering.

9.1.13 SEU, SEE, SEL

Single-event upset, single event effect, single-event latch-up. These effects are the result of the highly localised deposition of energy by single particles or their reaction products. The energy deposition is sufficient to cause observable effects.

9.2 Introduction: Overview of energetic particle radiation environment and effects

Radiation environments and effects shall be considered early in the design cycle. Energetic charged particles with energies in the MeV range are encountered throughout the Earth's magnetosphere, in inter-planetary space, and in the magnetospheres of other planets. At pre-phase A, radiation environments are an element in trade-offs for orbit selection. Effects on both the payload and on the spacecraft carrier shall be considered. A radiation environment specification for a mission shall be established wherein all types of radiation shall be considered, reflecting general and mission-specific radiation susceptibilities.

9.2.1 Environments

9.2.1.1 Radiation belts

Energetic electrons and ions are magnetically trapped around the earth forming the ***radiation belts***, also known as the Van Allen belts. The radiation belts are crossed by low altitude orbits as well as high altitude orbits (geostationary and beyond). The radiation belts consist principally of electrons of up to a few MeV energy and protons of up to several hundred MeV energy. The so-called ***south Atlantic anomaly*** is the inner edge of the inner radiation belt encountered in low altitude orbits. The offset, tilted geomagnetic field brings the inner belt to its lowest altitudes in the south Atlantic region. More information can be found in references [RD9.1, RD9.2].

9.2.1.2 Solar energetic particles

Energetic solar eruptions (***solar particle events*** - *SPEs*) produce large fluxes of solar energetic particles (SEPs) which are encountered in interplanetary space and close to the earth. The Earth's magnetic field provides a varying degree of geomagnetic shielding of near-Earth locations from these particles.

9.2.1.3 Galactic cosmic-rays

There is a continuous flux of galactic cosmic-ray (GCR) ions. Although the flux is low (a few particles /cm^2/sec), GCRs include energetic heavy ions which can deposit significant amounts of energy in sensitive volumes and so cause problems.

9.2.1.4 Other planets

The above environments are common to other planets than the Earth. Jupiter and Saturn, in particular, have severe radiation environments. Mercury also has a small magnetosphere.

9.2.1.5 Secondary radiation

Secondary radiation is generated by the interaction of the above environmental components with materials of the spacecraft. A wide variety of secondary radiations are possible, of varying importance.

9.2.1.6 Other radiation sources

Other sources of radiation include neutrons resulting from energetic particle interactions with the upper atmosphere and emissions from on-board radioactive sources such as in radioisotope thermo-electric generator (RTG) electrical power systems.

9.2.2 Effects survey

The above radiation environments represent important hazards to space missions. Energetic particles, particularly from the radiation belts and from solar particle events cause radiation damage to electronic components, solar cells and materials. They can easily penetrate typical spacecraft walls and deposit doses of hundreds of kilorads during missions in certain orbits.

Radiation is a concern for manned missions. Astronauts must operate within defined limits of dose equivalent [RD9.3], determined to ensure as low as reasonably achievable long-term risk. There are many possible radiation effects to humans, beyond the scope of this document. These are described in [RD9.4]. To account for dependence of effects on

particle species, energy and LET, dose is expressed as dose equivalent where energy, LET and species dependent factors are used to scale absorbed dose contributions. For example, heavy ions and neutrons are known to cause severe biological damage, and therefore these contributions receive a heavier weighting than gamma radiation. The “quality factors”, as they are called, are established by the International Commission on Radiological Protection [RD9.5].

Energetic ions, primarily from cosmic rays and solar particle events, lose energy rapidly in materials, mainly through ionization. This energy transfer can disrupt or damage targets such as a living cell, or a memory element, leading to single-event upset (SEU) of a component, or an element of a detector (radiation background).

SEUs and biological effects can also arise from nuclear interactions between very energetic trapped protons and materials (sensitive parts of components, biological experiments, detectors). Here, the proton breaks the nucleus apart and the fragments cause highly-localized ionization.

Energetic particles also interfere with payloads, most notably with detectors on astronomy and observation missions where they produce a `background' signal which may not be distinguishable from the photon signal being counted, or which can overload the detector system.

Energetic electrons can penetrate thin shields and build up static charge in internal dielectric materials such as cable and other insulation, circuit boards, and on ungrounded metallic parts. These can subsequently discharge, generating electromagnetic interference.

Apart from ionizing dose, particles can lose energy through non-ionizing interactions with materials, particularly through “displacement damage”, or “bulk damage”, where atoms are displaced from their original sites. This can alter the electrical, mechanical or optical properties of materials and is an important damage mechanism for electro-optical components (solar cells, opto-couplers, etc.) and for detectors, such as CCDs.

9.3 Quantification of effects and related environments

Models of the radiation environment are needed to assist in orbit selection, component selection and shielding optimization. In engineering a space system to operate in the space environment, it is necessary to relate the environment to system degradation quantitatively. This also involves questions of testing systems and their components for verification that they meet the performance requirements in the presence of the space environment.

For example, testing with calibrated radioactive sources can establish the threshold for functional failure or degradation of an electronic component in terms of *total absorbed dose* (often referred to simply as “total dose”, or just “dose”). Radiation environment models, used together with mission orbital specifications can predict the dose and enable correct performance to be verified.

The table below gives the parameters which shall be used for quantification of the various radiation effects.

Table 9-1: Parameters for quantification of radiation effects

Radiation effect	Parameter
Electronic component degradation	Total ionizing dose.
Material degradation	"
Material degradation (bulk damage)	Non-ionizing dose (NIEL).
CCD and sensor degradation	NIEL
Solar cell degradation	NIEL & *equivalent fluence.*
Single-event upset, latch-up, etc.	LET spectra (ions); proton energy spectra; explicit SEU/SEL rate of devices.
Sensor interference (background signals)	Flux above above energy threshold and/or flux threshold; explicit background rate.
Internal electrostatic charging	Electron flux and fluence; dielectric E-field.

Although some of these parameters are readily derivable from a specification of the environment, others either need explicit consideration of test data (for example single-event upset calculation) or the detailed consideration of interaction geometry and mechanisms (e.g. radiation background estimation).

In the following sections, the basic data on the environment are presented, along with models to be employed for deriving data beyond those presented. Effects and the specific methods for derivation of engineering quantities will then be presented.

9.4 Energetic particle radiation environment reference data, models and analysis methods

Figure 9-1 shows the ranges of electrons and protons in aluminium.

9.4.1 Trapped radiation belts

9.4.1.1 Basic data

Trapped radiation belt charged energetic particles gyrate in the geomagnetic field with a gyration period $t_c = 2\pi m/(eB)$ and a radius of gyration of $R_c = mv^2/(eB)$.

Table 9-2 gives typical characteristics of energetic particles:

Table 9-2: Characteristics of typical radiation belt particles

	Particle	
	1MeV Electron	**10MeV Proton**
Range in aluminium (mm)	2	0.4
Peak equatorial omni-directional flux ($cm^{-2}.s^{-1}$)*	4×10^{6}	3.4×10^{5}
Radial location (L) of peak flux (Earth radii)*	4.4	1.7
Radius of gyration (km)		
@ 500km	0.6	50
@ 20000km	10	880
Gyration period (s)		
@ 500km	10^{-5}	7×10^{-3}
@ 20000km	2×10^{-4}	0.13
Bounce period (s)		
@ 500km	0.1	0.65
@ 20000km	0.3	1.7
Longitudinal drift period (min)		
@ 500km	10	3
@ 20000km	3.5	1.1

* derived from the models of Section 9.4.1.2

9.4.1.2 Standard models

For trapped radiation, the standard models of radiation belt energetic particle shall be the AE-8 and AP-8 models for electrons [RD9.6] and protons [RD9.7] respectively. They were developed at the NSSDC at NASA/GSFC based on data from satellites flown in the '60s and early '70s. The models give omni-directional fluxes as functions of idealized geomagnetic dipole co-ordinates B/B_0 and L (see Clause 5). This means that they must be used together with an orbit generator and geomagnetic field computation to give instantaneous or orbit-averaged fluxes. The user must define an orbit, generate a trajectory, transform it to geomagnetic co-ordinates and access the radiation belt models to compute flux spectra. Apart from separate versions for solar maximum and solar minimum, there is no description of the temporal behaviour of fluxes. At high altitudes in particular (e.g.

around geostationary orbit) fluxes vary by orders of magnitude over short times and exhibit significant diurnal variations; the models do not describe these. In addition, the models do not contain any explicit flux directionality.

At low altitudes, on the inner edge of the radiation belts, particle fluxes rise very steeply with altitude and small errors in computing locations can give rise to large errors in particle fluxes. This is a problem since the geomagnetic field is shifting and decaying so that the situation is no longer the same as when the model data were acquired. Use of a geomagnetic field model other than the one used in generating the model can result in large flux errors at low altitude. The models shall only be used together with the geomagnetic field models shown in Table 9-3.

Table 9-3: Standard field models to be used with radiation-belt models

Radiation-belt Model	Geomagnetic Field Model
AE-8-MIN	Jensen-Cain 1960
AE-8-MAX	Jensen-Cain 1960
AP-8-MIN	Jensen-Cain 1960
AP-8-MAX	GSFC 12/66 extrapolated to 1970

Although use of an old field model and epoch can reduce errors in the magnitudes of fluxes, it should be noted that it does not model the spatial locations of radiation-belt features (e.g. the position of the south Atlantic anomaly), or particle fluxes, as they are today.

The particle ranges shown in Figure 9-1 show that in order to penetrate typical spacecraft shielding of the order of millimetres, protons need tens of MeV energies and electrons need in excess of about 0.5 MeV. The AP-8 model for protons gives proton fluxes from 0.1 to 400 MeV while the AE-8 model for electrons covers electrons from 0.04 to 7 MeV. Figure 9-2 shows contour plots of AE-8 and AP-8 model omnidirectional, integral fluxes for energies above 1 and 10 MeV respectively in idealised dipole space.

Figure 9-3 shows values of energetic electron and proton particle fluxes as stored in these models, for positions on the geomagnetic equator ($B=B_0$), as functions of L for both solar maximum and solar minimum. This shows that as far as the models are concerned, the solar activity only affects electron fluxes in the mid-L range and protons at low altitude where the higher neutral atmospheric density at solar maximum leads to reduced proton fluxes because of enhanced loss. Solar cycle effects on electrons appear to differ from this behaviour in reality [RD9.8]

9.4.1.3 The south Atlantic anomaly

The south Atlantic anomaly (see Section 9.2.1.1) produces an “island” of radiation and provides the only significant radiation encountered on low earth orbits with altitudes below about 800km and inclinations below about 40°. Figure 9-4 shows the south Atlantic anomaly at 400km.

Anisotropy (the “East-West Effect”)

Because of the inclination of geomagnetic field-lines with respect to the atmosphere here, particles reaching a point from the West have gyrated from higher altitude while those arriving from the East have gyrated from lower altitude. There are fewer coming from below because of atmospheric absorption and therefore an asymmetry in the fluxes results. This can be important in certain cases, including the International Space Station Alpha. The current standard AP-8 model does not treat this effect but models have been developed by NASA [9.9] and BIRA-IASB [RD9.10]. Figure 9-5, from the BIRA-IASB ANISO model, shows the integral orbit-averaged flux of 100MeV protons in the horizontal plane as a function of look-direction relative to North. The east and west “lobes” are clear. The ratio of the East and West peak fluxes is about 4.6. Measurements from MIR are also available which are consistent with this ratio [RD9.11].

Location of the South Atlantic Anomaly

The slow movement of the south Atlantic anomaly as a result of shifts in the geomagnetic field has been clearly observed and agrees with expectation. This shift is essentially Westward at a rate of 0.3^{o} per year (~10° since the models were created) and account shall be taken of this figure for low earth orbits when planning operations which involve a sensitivity to radiation (e.g. payload radiation background, astronaut EVA). Models including this shift capability are available [RD9.12].

9.4.1.4 Dynamics of the outer radiation belt

The dynamic nature of the outer electron radiation belt, together with its diurnal variations mean that unless one is interested in long-term averages (such as provided by AE-8), some statistical description is desirable. This is especially true when deep dielectric charging and radiation background are of concern. No standard models for the variability are yet available, but for engineering purposes the CRRESELE model may be used [RD9.13]. An older version of the AE-8 electron model, AE-4 [RD9.14], included a statistical model giving standard deviations of the logarithm of electron fluxes (assumed to be normally-distributed). It also included a model for local time flux modulation. This was a sinusoidal model providing amplitudes of the variation, with a fixed maximum at 11:00 local time. These have been extended and applied to the AE-8 model [RD9.15], although this extension is unvalidated.

9.4.2 Solar particle event models

9.4.2.1 Standard model for mission-integrated fluences

During energetic events on the sun, large fluxes of energetic protons are produced which can reach the Earth. Solar particle events, because of their unpredictability and large variability in magnitude, duration and spectral characteristics, have to be treated statistically. However, large events are confined to a 7-year period defined as solar maximum. Although large events are absent during the remaining 4 solar minimum years of the 11-year solar cycle [see Clause 6] the occasional small event can still occur.

Figure 9-6, based on data from Ref. [RD9.16], shows reference data for solar maximum solar proton fluences at various energy levels based on the JPL-1991 model. The data are also tabulated in Table 9-4.

This statistical model is based on data from 3 solar cycles. This shall be the standard model used for engineering consideration of time-integrated effects. Since this is a statistical model, a probability level must be entered. On the basis of analysis of worst-case periods [RD9.17], the following probability levels are recommended:

The JPL model provides data up to 60MeV. For fluences at energies above this, an exponential fit to the rigidity spectrum shall be used, where rigidity is defined as:

$$P = (A/Z)\,(E^2 + 1862\,E)^{1/2}/10^3$$

where P is in GV and E is in MeV.

Table 9-4: Fluence levels (/cm^2) for energy, mission duration and confidence levels from the JPL-1991 model

Energy (MeV)	Probability (confidence) level (%)	1 year	2 years	3 years	5 years	7 years
>1	50	5.92×10^{10}	1.16×10^{11}	1.72×10^{11}	3.15×10^{11}	3.99×10^{11}
>1	75	8.76×10^{10}	1.74×10^{11}	2.42×10^{11}	3.87×10^{11}	4.77×10^{11}
>1	90	1.26×10^{11}	2.39×10^{11}	3.25×10^{11}	4.79×10^{11}	5.89×10^{11}
>1	95	1.64×10^{11}	2.92×10^{11}	3.96×10^{11}	5.55×10^{11}	6.95×10^{11}
>1	99	2.91×10^{11}	4.52×10^{11}	5.89×10^{11}	7.68×10^{11}	1.00×10^{12}
>4	50	8.00×10^{9}	2.02×10^{10}	3.33×10^{10}	5.75×10^{10}	8.84×10^{10}
>4	75	1.69×10^{10}	3.58×10^{10}	5.74×10^{10}	9.28×10^{10}	1.27×10^{11}
>4	90	3.46×10^{10}	6.42×10^{10}	9.81×10^{10}	1.49×10^{11}	1.96×10^{11}
>4	95	5.49×10^{10}	9.54×10^{10}	1.40×10^{11}	2.09×10^{11}	2.70×10^{11}
>4	99	1.50×10^{11}	2.28×10^{11}	3.10×10^{11}	4.45×10^{11}	5.63×10^{11}
>10	50	2.11×10^{9}	5.59×10^{9}	9.83×10^{9}	1.79×10^{10}	2.78×10^{10}
>10	75	5.34×10^{9}	1.18×10^{10}	1.85×10^{10}	3.16×10^{10}	4.70×10^{10}
>10	90	1.25×10^{10}	2.42×10^{10}	3.41×10^{10}	5.28×10^{10}	7.55×10^{10}
>10	95	2.12×10^{10}	3.79×10^{10}	5.19×10^{10}	7.51×10^{10}	1.05×10^{11}
>10	99	5.88×10^{10}	1.02×10^{11}	1.31×10^{11}	1.86×10^{11}	2.36×10^{11}
>30	50	4.50×10^{8}	1.28×10^{9}	2.22×10^{9}	4.56×10^{9}	6.61×10^{9}
>30	75	1.23×10^{9}	2.94×10^{9}	4.67×10^{9}	8.33×10^{9}	1.16×10^{10}
>30	90	3.19×10^{9}	6.71×10^{9}	1.00×10^{10}	1.66×10^{10}	2.24×10^{10}
>30	95	5.81×10^{9}	1.13×10^{10}	1.66×10^{10}	2.63×10^{10}	3.52×10^{10}
>30	99	1.93×10^{10}	3.49×10^{10}	4.83×10^{10}	6.96×10^{10}	9.04×10^{10}
>60	50	1.67×10^{8}	4.92×10^{8}	9.18×10^{8}	1.73×10^{9}	2.85×10^{9}
>60	75	4.93×10^{8}	1.24×10^{9}	2.11×10^{9}	3.52×10^{9}	5.26×10^{9}
>60	90	1.37×10^{9}	2.83×10^{9}	4.39×10^{9}	7.00×10^{9}	1.01×10^{10}
>60	95	2.61×10^{9}	4.92×10^{9}	7.36×10^{9}	1.12×10^{10}	1.53×10^{10}
>60	99	9.20×10^{9}	1.62×10^{10}	2.26×10^{10}	3.27×10^{10}	4.25×10^{10}

Table 9-5: Standard probability (confidence) levels to be applied for various mission durations

Number of years of exposure	Probability level (%)
1	97
2	95
3	95
4	90
5	90
6	90
7	90

9.4.2.2 Spectrum of individual events

The August 1972 event produced a peak flux near the Earth in excess of 10^6 protons.cm^{-2}.s^{-1} above 10MeV energy, while the October 1989 event produced a peak flux of about 10^5

protons.cm^{-2}.s^{-1}. A fluence spectrum which is often used to represent a worst-case flare, classified as `anomalously large' is based on the very large August 1972 event:

$$J(E) = 7.9 \times 10^{9} \exp \{ \{30-E\} / \{26.5\} \}$$

with energy E in MeV and fluence J in protons.cm^{-2}. The October 1989 event was the largest seen since August 1972 but had lower fluences at the medium energies. A fit to its *differential* fluence spectrum is given by a three-part power law:

$$j(E) = \begin{cases} 1.2 \times 10^{11} E^{-1.7} & \text{for } E<30\text{MeV} \\ 4.5 \times 10^{12} E^{-2.8} & \text{for } 30\text{MeV}<E<150\text{MeV} \\ 5.5 \times 10^{9} E^{-1.45} & \text{for } E>150\text{MeV} \end{cases}$$

where E is in MeV and j is in protons.cm^{-2}.MeV^{-1}.

Comparison of these two spectra reveals important points. Since flare spectra are variable, the worst-case event at one energy is not necessarily worst-case at another. The August 1972 event yield worst-case doses at most typical spacecraft shielding (1-10mm) where particles of energy 10-70 MeV are most important. The October 1989 flare is apparently more severe at lower and higher energies. Lower energies are important for surface material and solar cell effects and the higher energies more important for nuclear interactions giving rise to certain types of background and single-event upsets. So the term "worst-case" is application dependent.

9.4.2.3 Event probabilities

Burrell, as reported in [RD9.18], developed a modified Poisson statistic to describe the probability p of a number of events n occurring during a time t, based on a previously observed frequency of N during time T:

$$p(n,t; N,T) = \{(n+N)! \, (t/T)^{n}\} / \{n!N! \, (1+t/T)^{N+n+1}\}$$

In this equation, N=1 and T=7 for the anomalous class of flare, while for ordinary flares, N=24 and T=7. This is sometimes useful in considering numbers of events in contrast to the total fluence. Simple application of Poisson statistics is also useful.

9.4.2.4 Analysis of event records

The JPL-91 model provides data only for integrated effects analysis (dose, long-term degradation, total upset count, etc.). It is often necessary to consider instantaneous fluxes. For radiation background estimation for example, the fluxes are required above an energy threshold determined by sensor shielding and sensor sensitivity, and above a flux threshold determined by sensor signal-to-noise characteristics. Two reference environment data resources are available: the NASA OMNIWEB database [RD9.19], and the NOAA GOES [RD9.20] database. With these databases, the durations and magnitudes of events above energy and flux thresholds can be analyzed. Both databases are available on the WWW and provide a comprehensive long-term database of measurements of the interplanetary environment. OMNIWEB contains a complete database of energetic proton data from the IMP series of spacecraft. The NOAA GOES satellites have returned energetic proton and electron data from geostationary orbit since January 1986. Further information is provided in Annex G.

9.4.2.5 Solar particle event ions

For analysing single event upset rates during solar particle events (SPE's), the CREME96 model shall be used. It can also be used for other applications where data on severe SPE conditions are needed, such as background estimation. CREME96 is described further in Section 9.4.3. While the older CREME model contained models for the peak flux for various types of events, CREME96 contains models based on the October 1989 event. It provides models of energy spectrum, composition and LET spectrum for the worst week, worst day and peak 5 minutes. The older CREME model provided more choice of peak environments. However, some of the more severe options were unrealistic.

9.4.2.6 Other models

Other model developments, which may lead to updates of this Standard, are discussed in Annex G. These developments relate to alternative statistical approaches and models for peak fluxes.

9.4.2.7 Directionality

Fluxes and fluences of solar energetic particles shall be assumed to be isotropic in interplanetary space. This may not be true in near-Earth space due to geomagnetic shielding (see Section 9.4.4).

9.4.3 Cosmic ray environment and effects models

Cosmic-Ray environment and effects models were originally created by Adams and co-workers at the U.S. Naval Research Laboratory [RD9.21], under the name CREME. They provided a comprehensive set of cosmic ray and flare ion LET and energy spectra, including treatment of geomagnetic shielding and material shielding. CREME also included upset rate computation based on the path-length distribution in a sensitive volume and also treated in a simple manner trapped proton-induced SEUs. CREME has been superseded by CREME96 [RD9.22]. The major differences are in the inclusion of a model of the cosmic ray environment and its solar-cycle modulation due to Nymmik et al. [RD9.23], improved geomagnetic shielding calculation, improved material shielding calculation and more realistic solar energetic particle event (SEPE) ion environments (see Section 9.4.2.5). Cosmic ray fluxes are anti-correlated with solar activity so the highest cosmic ray fluxes occur at solar minimum. CREME96 shall be the standard model for cosmic ray environment assessment. It shall also be the standard for evaluation of single event effects from cosmic rays, from solar energetic particles and from energetic protons.

Figure 9-7 shows composite LET spectra for three CREME96 environments: the nominal solar minimum cosmic ray flux; the average flux for a "worst week" of a large SEPE; and the peak flux from a large SEPE. Three orbital situations, with different geomagnetic shielding, are shown: geostationary (which also applies to high altitudes and interplanetary), a polar orbit (900km) and LEO (28^o, 450km). Ions from Z=1 to 92 shall be included and, in the absence of a reason to use another value, shielding of $1 g/cm^2$ aluminium shall be assumed.

9.4.3.1 Directionality

Fluxes and fluences of solar energetic particles shall be assumed to be isotropic in interplanetary space. This may not be true in near-Earth space due to geomagnetic shielding (see Section 9.4.4).

9.4.4 Geomagnetic shielding

The Earth's magnetic field partially shields near-earth space from solar energetic particles and cosmic rays, an effect known as geomagnetic shielding. However, these particles can easily reach polar regions and high altitudes such as the geostationary orbit. Geomagnetic shielding of protons is computed on the basis of the trajectory in geomagnetic *B*, *L* space (see Clause 5).

At a given location in the field there will be minimum cut-off energies necessary for ions to penetrate to that point. Størmer's theory gives a cut-off rigidity, P_c, for particle arrival at a point, depending on the point's geomagnetic *R*, l co-ordinates (see Clause 5) and the angle of ion arrival from east, g [RD9.24]:

$$P_c = \{ M \cos^4 l \} / \{ R^2 [1 + (1 - \cos^3(l) \cos(g))^{1/2}]^2 \}$$

M is the normalized dipole moment of the Earth. From this equation, it can be seen that cosmic-rays penetrate the geomagnetic field more easily from the west ($g=180^o$) than from the east ($g=0$). The *R*, λ co-ordinates can be computed from *B* and *L* according to the method of Roberts [RD9.25]. For vertical arrival, the expression simplifies to:

$$P_c \sim= 16 \cos^4(\lambda) / R^2 = 16 / L^2 \text{ GV},$$

since g=90° and $R = L \cos^2(\lambda)$.

An approximate value of 16 for the constant $M/4$ is used to fit with observed *effective* cut-offs. Magnetospheric disturbances, which often follow solar-flares and/or CME's, can result in a lowering of cutoff; this has been described by Adams et al. [RD9.24] as:

$$\Delta P_c / P_c = 0.54 \exp(- P_c /2.9) \text{ with } P_c \text{ in units of GV.}$$

Stassinopoulos and King [RD9.26] developed a model which has total cut-off at L=5. It assumes that no protons can penetrate to lower L values. It can be shown that this model corresponds to a quiet magnetosphere vertical cut-off model excluding protons of E<200MeV from L<5 R_E This model is adequate for most cases. However, in reality protons of lower energy can penetrate below L=5 with non-vertical arrival directions, especially in a disturbed magnetosphere where the geomagnetic shielding is weakened. For westward arrival at the L=5 geomagnetic equator in a disturbed magnetosphere, the energy cut-off could be as low 30MeV.

For engineering purposes, geomagnetic cutoff shall not be applied to orbits spending more than 50% of the orbit period above L=5. Geomagnetic cut-off shall always be applied to orbits spending more than 75% of their time below L=5.

9.4.5 Spacecraft secondary radiation

For engineering purposes it is often only electron-induced bremsstrahlung radiation that is considered as a significant secondary source. In special cases other secondaries need to be considered.

In evaluating the radiation background effects in detector systems, it is often secondary radiation that is important. This might be because of heavy shielding removing primaries, veto systems which actively protect against counting primary-induced signals, or secondary radiation generated within the sensing band of an instrument. Most secondary radiation is emitted at the instant of interaction ("prompt") while some is emitted some time after a nucleus has been excited by an incoming particle (induced radioactivity).

In manned missions, secondary neutrons and other products can be important contributors to the radiological hazard.

By its nature, secondary radiation has to be analysed on a case-by-case basis, possibly through Monte-Carlo simulation. For engineering estimates of bremsstrahlung, the SHIELDOSE model shall be used (see Section 9.5.1).

9.4.6 Neutrons

A low-level flux of neutrons of between 0.5 $cm^{-2}.s^{-1}$ and 4 $cm^{-2}.s^{-1}$ is present at low altitudes due to cosmic ray interactions with the atmosphere. Neutrons are also generated by energetic particles undergoing nuclear interactions with the material of spacecraft. These neutrons have to be considered for manned missions. They also play a role in generating background in sensitive detector systems.

9.5 Analysis methods for derived quantities

The following analysis methods shall be used.

The environment models specified in 9.4 shall be used to generate the primary data described in Section 9.3. The secondary data shall be derived as follows:

9.5.1 Ionizing dose:

The ionizing dose environment is represented by the dose-depth curve. This may provide dose as a function of shield thickness in planar geometry or as a function of spherical shielding about a point. The planar model is appropriate for surface materials or for locations near to a planar surface. In general, electronic components are not in such locations and a spherical model is recommended for general specification.

The SHIELDOSE model shall be used [RD9.27] for ionizing dose. Alternatively, a method which has been validated with respect to SHIELDOSE may be used. This method

uses a pre-computed data-set of doses from electrons, electron-induced bremsstrahlung and protons, as derived from Monte-Carlo analysis. The doses are provided as functions of material shielding and incident electron and proton energy. The actual spectrum is folded with this data-set to yield the dose at a given depth, *d* :

$$D(d) = \sum_E f(E) \,.\, \mathrm{D}(E,d)\, \Delta E$$

Figure 9-8 shows this data-set. A computerized version of this procedure is available as described in Annex G.

The reference geometrical configuration for the dose-depth curve shall be a solid aluminium sphere. The SHIELDOSE dataset represents a planar medium and the conversion is performed as follows [RD9.27]:

$$D_{\mathrm{Sphere}} = 2D_{\mathrm{Plane}} \left\{ 1 - \frac{\mathrm{d}(\log D_{\mathrm{Plane}})}{\mathrm{d}(\log d)} \right\}$$

This conversion is included in the computer version.

In cases where more careful analysis of the shielding of a component or of other sensitive locations is necessary, a sectoring calculation is often performed. This might be necessary if the doses computed from simple spherical shielding are incompatible with the specification of the allowable radiation dose. The sectoring method traces rays from the point of interest through the shielding in a large number of directions. Along each direction the derived shielding, together with the data on dose as a function of shielding depth, *d*, is used to find the omnidirectional 4π dose contribution, $D_i(d)$, from each direction, *i*. The contributions, weighted by the solid angle increment around the rays, W_i, are then summed:

$$D_{\mathrm{tot}} = \sum_i (W_i/4\pi) \,.\, D_i(d)$$

If this procedure is used, it shall employ the spherical model for the dose-depth curve.

In some cases, it is efficient to derive a shielding distribution. This is the result of the ray-tracing described above and provides the distribution of encountered shielding $p(d)$. This distribution can be folded with the dose depth curve to derive the total dose. The advantage of this method is that various dose calculations can be efficiently performed for one geometry as represented by the shielding distribution.

It is important to recognise that a shielding analysis in the presence of significant anisotropies (e.g. as in Section 9.4.1.3) in the environment can result in serious error if the environment is assumed to be isotropic. This assumption is implicit in the sectoring method defined above since all directional contributions are derived from a common "omnidirectional" dose-depth curve.

9.5.2 Reference orbital dose data

Figure 9-9 shows a summary of expected doses on circular equatorial orbits as a function of the orbit altitude, based on the standard models described in Section 9.4. A spherical shield of 4mm aluminium is assumed.

Figure 9-10 shows a summary of the doses expected for a selection of common orbit types, based on the standard models. A 1 year mission and spherical aluminium shielding of 4mm radius is assumed. Dose from one years' accumulated solar energetic protons is also shown, with a confidence level of 95% that higher dose will not be seen. More details of the doses are given in Figure 9-11 in the form of doses as functions of the radius of the aluminium shielding.

9.5.3 Single-event upset rate

The CREME/CREME96 method shall be used [RD9.21, RD9.22]. It is possible to make upset rate predictions only when details of the device under consideration are known, particularly the critical charge and the sensitive volume dimensions. If a device is uncharacterized, tests shall be performed.

The test data shall show the normalized upset rate as a function of ion LET in the range 1 to 100 MeV.cm^2/mg and as a function of proton energy in the range 20-100MeV. These

data shall be used to make an estimate of the upset rate from trapped protons and solar protons using the two-parameter Bendel method [RD9.28], and of upsets due to galactic and solar ions using the method of CREME/CREME96. This latter shall be modified to account for the non-ideal upset rate as a function of ion LET derived from component test data [RD9.29] (the so-called "IRPP" method) as described below. This method has been implemented in CREME96. CREME96 also includes the two-parameter Bendel method. Alternative methods which have been thoroughly validated with respect to these methods may be applied.

To compute an upset rate for an electronic device or a detector from the predicted fluxes, device characteristics must be specified, particularly the size of the sensitive volume and the *critical charge*, or equivalently, critical energy E_c, in the volume which results in upset or registers as a "count".

For SEUs resulting from direct ionization the rate is found by integrating over the composite differential ion LET (L) spectrum, $f(L)$, and the distribution of path-lengths (l) for the sensitive volume, $p(l)$ [RD9.21, RD9.29]:

$$U = S/4 \int_{Ec/L\max}^{l\max} p(l) \int_{Ec/l}^{L\max} f(L)\, dL\, dl$$

which approaches $FS/4$ in a very sensitive detector (where E_c is very small, so all particles cause upset). S is the total surface area of the sensitive volume and F is the integral omnidirectional flux. Normally, for electronic components, the limiting solution does not apply and the integral must be evaluated. The integration limits are set by the sensitive volume dimensions and the critical energy E_c; E_c/L_{max} is the shortest path capable of supporting upset, l_{max} is the maximum pathlength, E_c/l is the minimum particle LET necessary to cause upset on a pathlength l and L_{max} is the maximum LET of the spectrum. Predicted upset rates are very sensitive to the integration limits, which are established through testing. This sensitivity is a result of the fact that particle fluxes in the environment are strong functions of LET. This form for the upset calculation assumes that above a unique critical charge, all bits, of equal size, will upset. Testing shows that in general the upset cross-section (σ, rate ÷ fluence) rises more gradually to a saturation cross-section, σ_0, and a method of calculation accounting for this is to sum a step-wise set of differential upset-rate calculations:

$$U = \sum_i (\sigma_i / \sigma_0)\, (\Delta U/\Delta L)_i\, \Delta L = \sum_i (\sigma_i / \sigma_0)\, \Delta U_i$$

where each U_i is calculated using the respective (σ_i and L_i)

An estimate of the upset rate from nuclear interactions of energetic protons can be obtained by integration of the product of the measured proton-induced upset cross section $\sigma(E)$ and the differential proton flux $f(E)$ over all energies. $\sigma(E)$ can be derived directly from the test data, or the 2-parameter Bendel fit can be used. Simulations of proton nuclear interactions can also be used to derive $\sigma(E)$, when data from heavy-ion testing is available to provide the critical charge and sensitive volume dimensions [RD9.28].

9.5.4 Solar cell degradation

The EQUFRUX-Si or EQFRUX-Ga models shall be used for silicon and gallium arsenide solar cell degradation calculations respectively [RD9.30]. In the absence of other test data, it shall be assumed that 10MeV protons cause equivalent damage to 3000 1 MeV electrons in silicon cells. Similarly it shall be assumed for gallium arsenide cells that the damage equivalence of a 10MeV proton is 400, 1000 and 1400 1 MeV electrons for short-circuit current, maximum power and open-circuit voltage degradation respectively. Since the default in these models is the assumption of infinite rear-side shielding of cells, this shall be the standard way of reporting results. However, account shall then be explicitly taken of radiation penetration though the rear-side of solar arrays.

9.5.5 Internal electrostatic charging

Engineering methods for specifying derived parameters related to internal electrostatic charging are currently under development and are described in Annex G. The flux of energetic electrons is clearly important, as are the energy spectrum and the duration of high-flux conditions. In addition, the "target" material plays a role and shielding of the target material obviously has a large effect.

9.5.6 Dose-equivalent

Dose equivalent calculation, for astronaut hazard estimation shall employ the quality factors defined in document [RD9.5]. For ions, the quality factor Q depends on the ion LET, L, as shown in Figure 9-12. Dose-equivalent is derived from:

$$D_{eq} = \sum D.Q(L)$$

where the sum is over all energies and radiation types. Electrons and gamma-rays have Q of 1. Protons have a Q of between 1 and 5 (the latter because of the nuclear interaction effects). Neutrons have Q between 5 and 20, depending on energy [RD9.5].

9.5.7 Non-ionizing dose

Damage to CCDs and other electro-optical components susceptible to displacement damage shall employ the NIEL function, N(E) [RD9.31], shown in Figure 9-13, to derive a 10MeV equivalent proton damage fluence F_D:

$$F_D = \sum_E f(E).\, N_{10}(E)\, .\, \Delta E$$

or a non-ionizing dose, D_N:

$$D_N = \sum_E f(E).\, N(E)\, .\, \Delta E$$

where: $f(E)$ is the differential fluence spectrum

$N(E)$ is the NIEL function

$N_{10}(E)$ is the NIEL function normalised to 10MeV

ΔE is the energy step of the sum.

9.6 Tailoring guidelines: orbital and mission regimes

In this section, attention is drawn to special considerations for various orbit types.

9.6.1 Geostationary orbit

Geostationary orbit is a circular orbit usually encountering an environment dominated by energetic electrons. This environment is characterized by strong time variations with many extended quiet periods of low radiation levels and many episodes of intense injections of energetic electrons which increase dose, sensor interference, electrostatic charging, etc. Solar protons and cosmic rays have unrestricted access to this orbit. Solar particles make short-lived but important contributions to the total dose, interference and single event effects. They do not directly participate in charging processes. Cosmic rays provide a continuous source of single-event effects and sensor interference.

9.6.2 MEO, HEO

These orbits encounter the electron-dominated environment mentioned above, but in addition, encounter the inner, proton radiation belt. In such orbits, single-event effects from protons and proton non-ionizing damage need to be considered. These orbits often encounter more severe electron environments, near the peak of the electron belt (the location of which is also variable) than geostationary orbit and so electrostatic charging can be a more serious threat.

9.6.3 LEO

For the foreseeable future, manned activities will be limited to low altitude (<550km) and medium-inclination (~55^o) orbits. We refer to these orbital regimes as LEO. Missions in

these orbits encounter the inner edge of the radiation belt. This region is dominated by the South Atlantic Anomaly. Also important is the strong asymmetry in fluxes from East and

The specification shall take account of the evolution of the mission orbit, either naturally or deliberately. This can have significant effects on radiation-belt exposure (e.g. due to natural perigee rise and apogee fall).

Operations which result in geo-synchronisation of the orbit shall be considered (e.g. geostationary, apogee longitude maintenance of near-synchronous HEO orbits). In such missions radiation belt exposures are not averaged out.

9.8 Figures

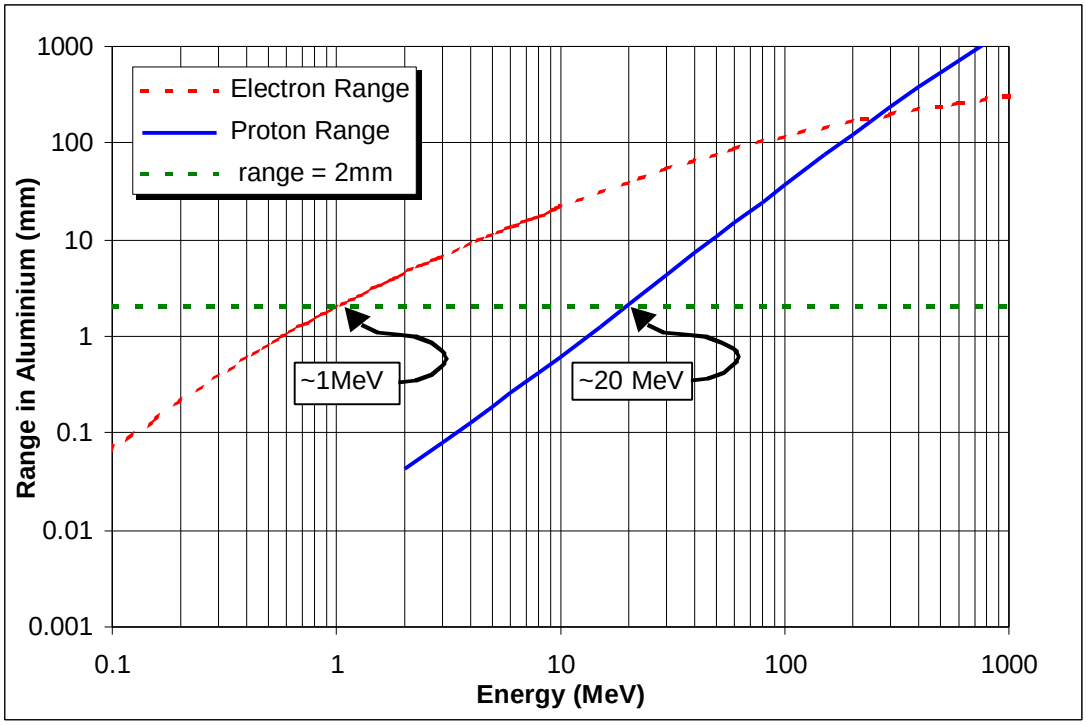

Figure 9-1 Mean ranges of protons and electrons in aluminium.

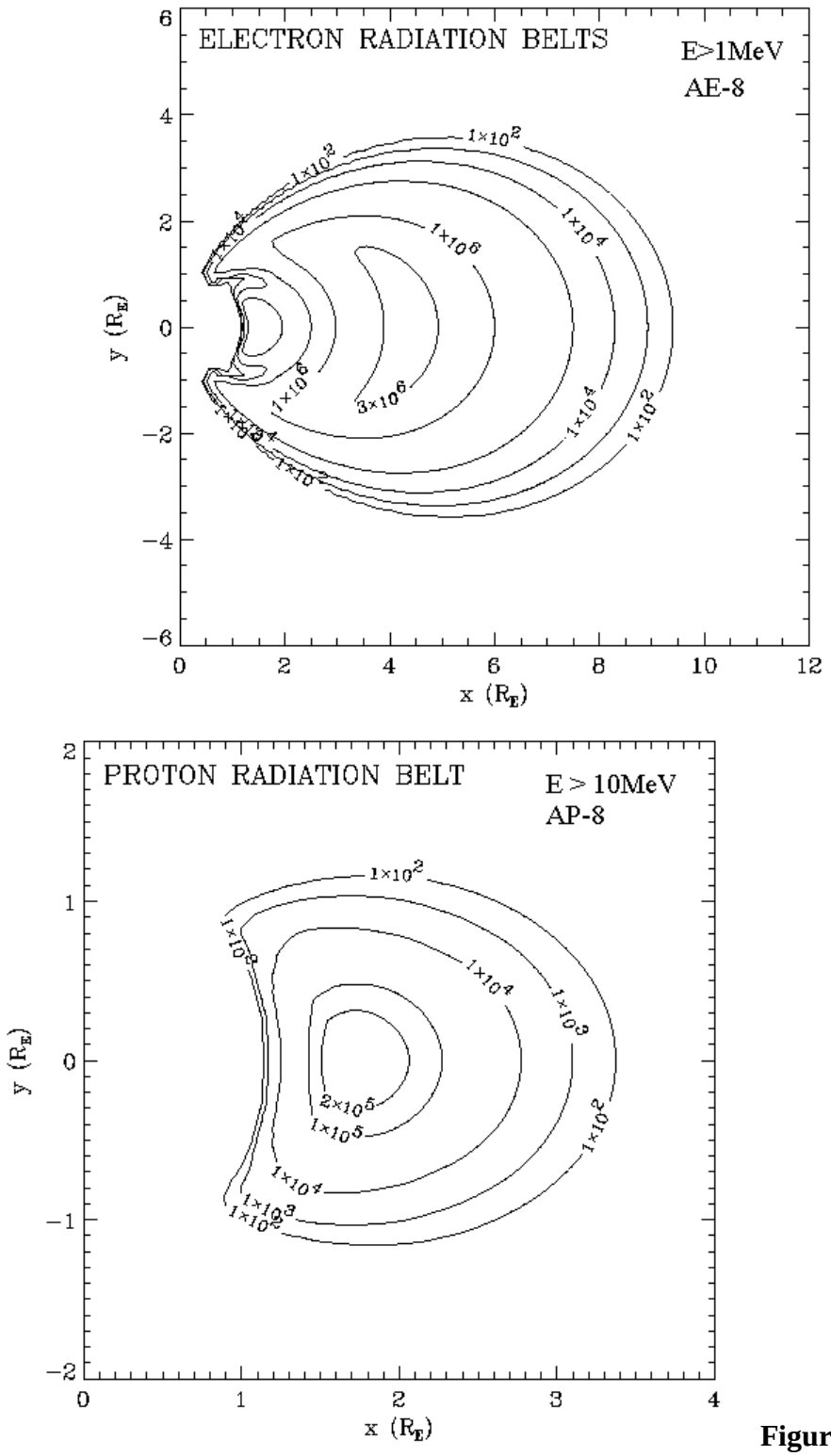

Figure 9-2 Contour plots of the electron and proton radiation belts. Omnidirectional fluxes are for particles > 1MeV and >10MeV respectively. The data are derived from the AE-8 and AP-8 models respectively and are shown in an ideal dipole representation of the earth's field.

(a)

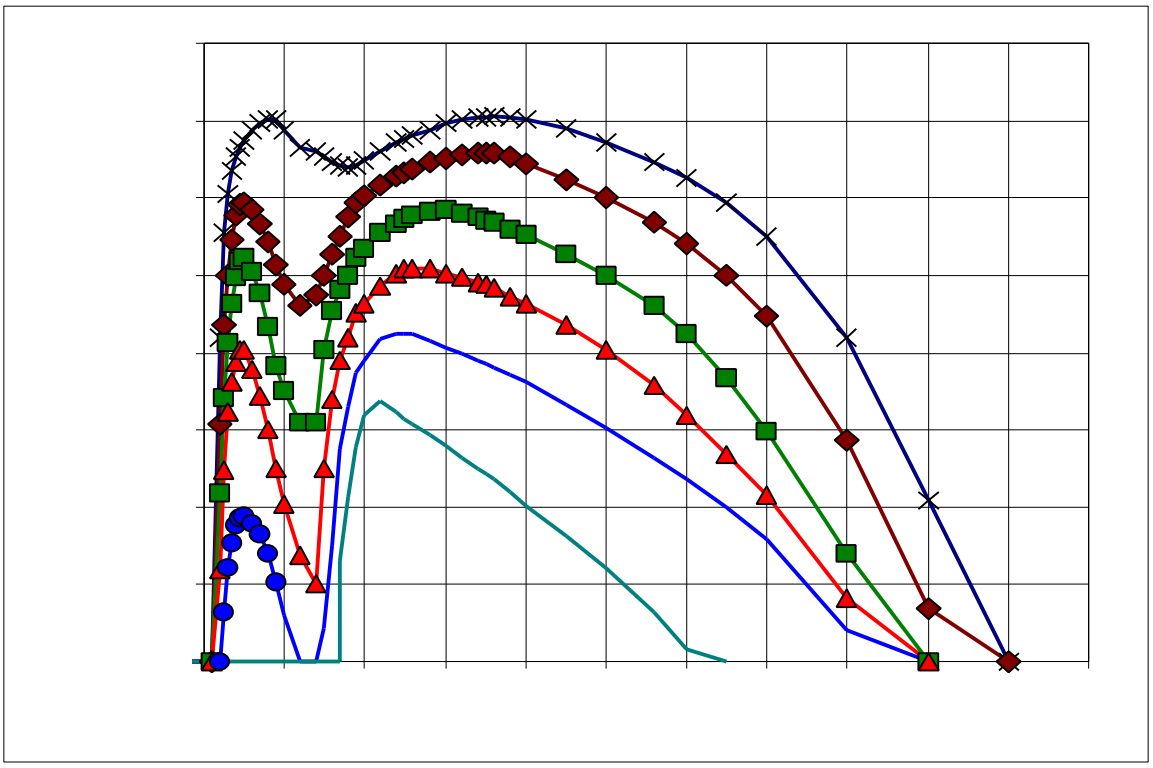

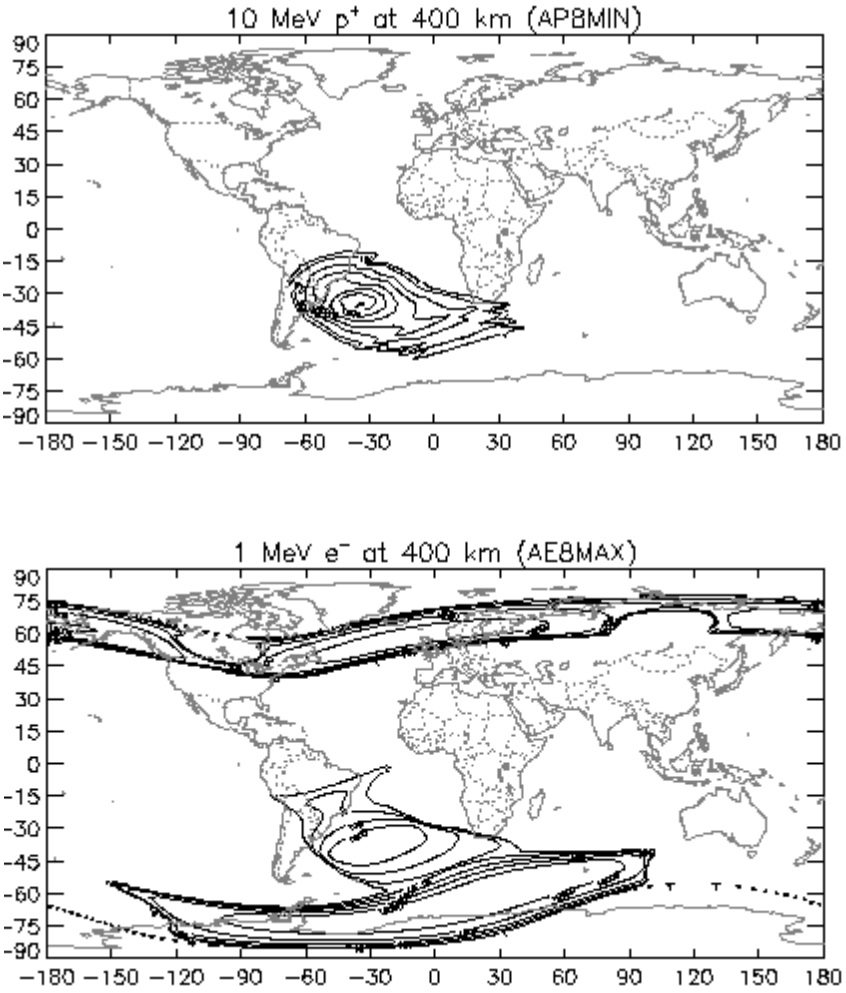

Figure 9-4 Integral omnidirectional fluxes of protons (>10MeV) and electrons (>1MeV) at 400km altitude showing the inner radiation belt's "South Atlantic Anomaly" and, in the case of electrons, the outer radiation belt encountered at high latitudes.

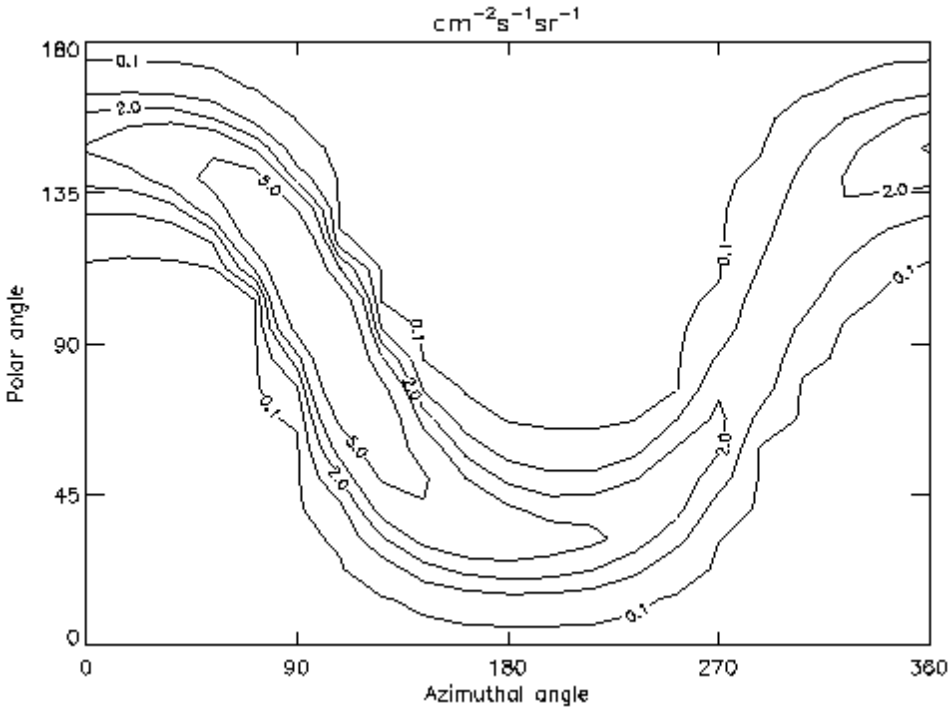

Figure 9-5 The flux anisotropy in low earth orbit averaged over an orbit of the space station for protons >100MeV energy. Polar and azimuthal angles are with respect to Zenith and North respectively. (Therefore the horizontal plane has polar angle 90^{o}, and westward viewing has azimuthal angle 90^{o})

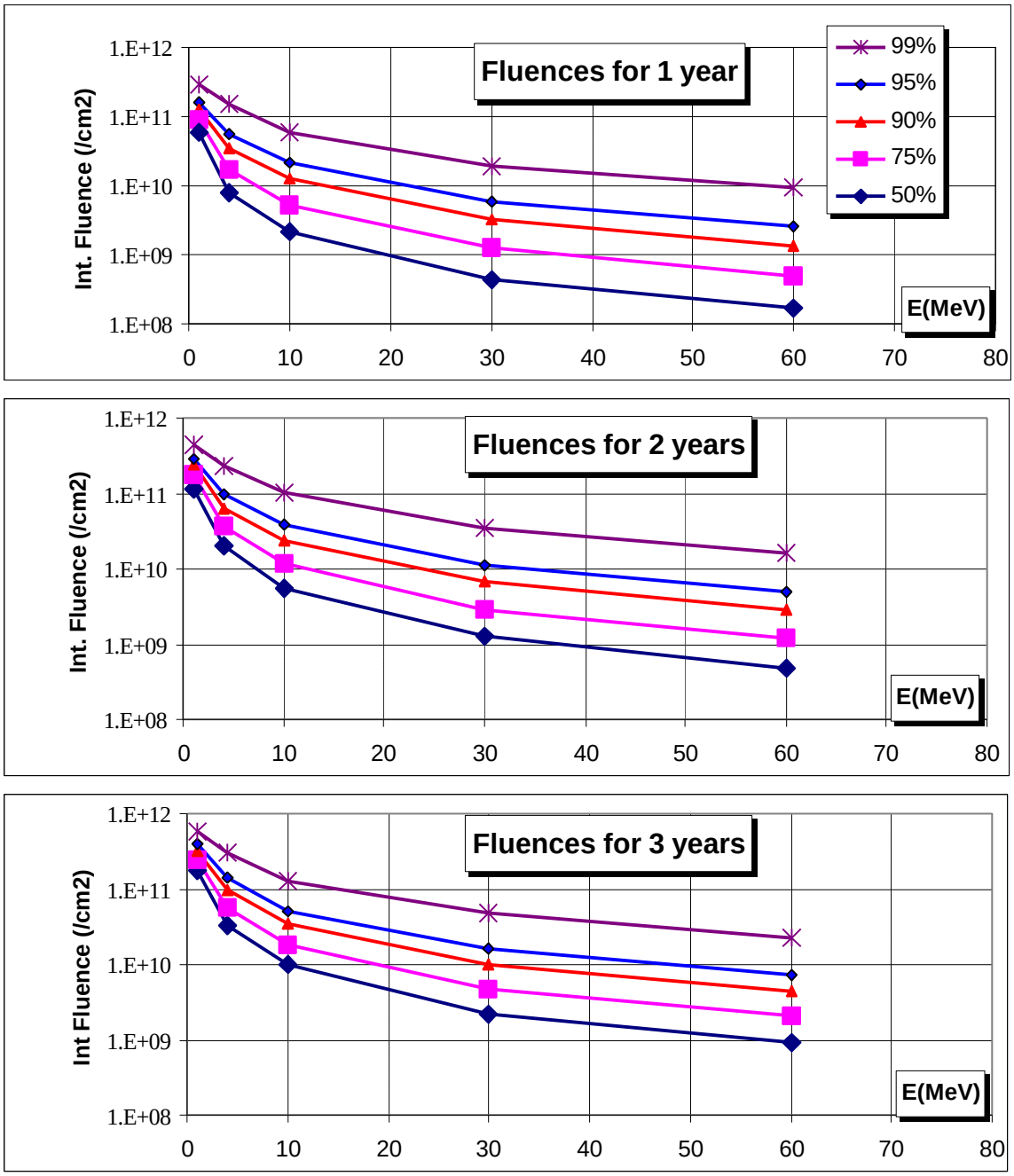

Figure 9-6 Solar proton fluence spectra for various statistical confidence levels (99%, 95%, 90%, 75% and 50%, from top to bottom in each panel) for various mission durations. (Data from JPL-1991 Model)

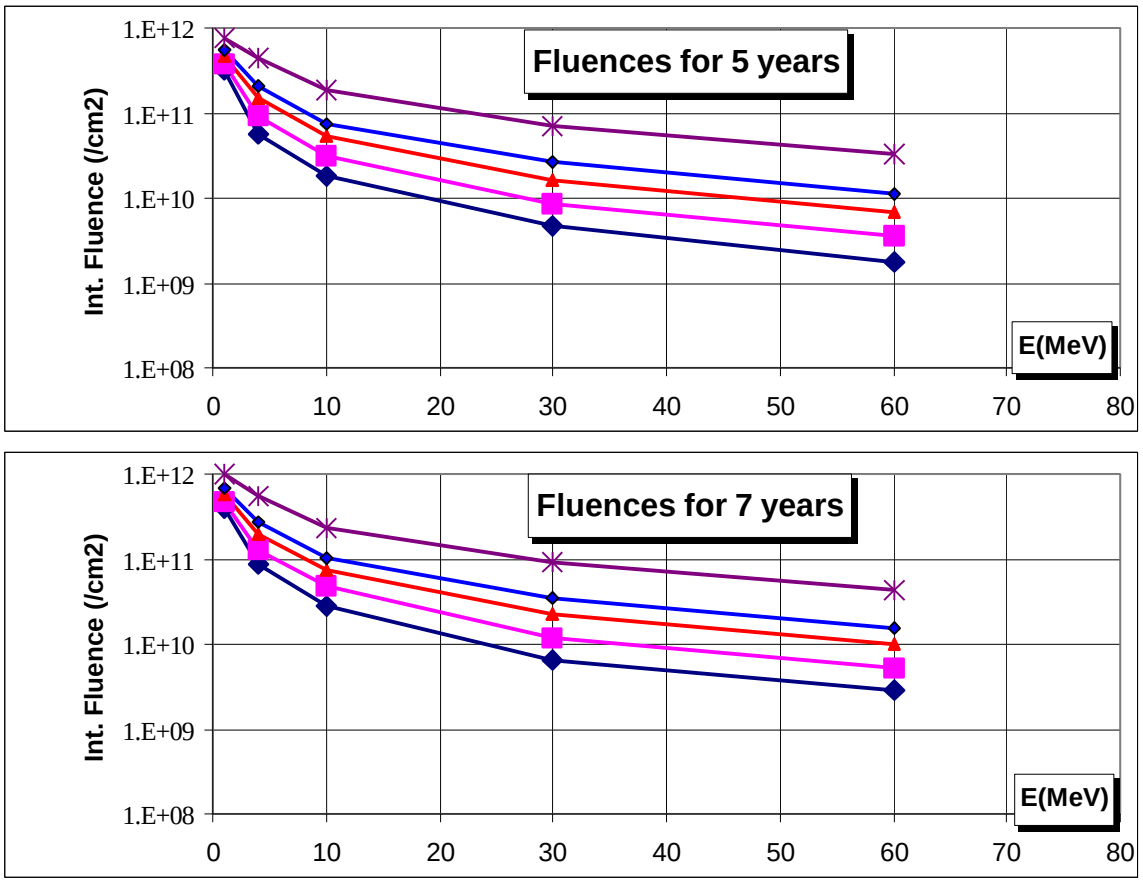

Figure 9-6 (continued)

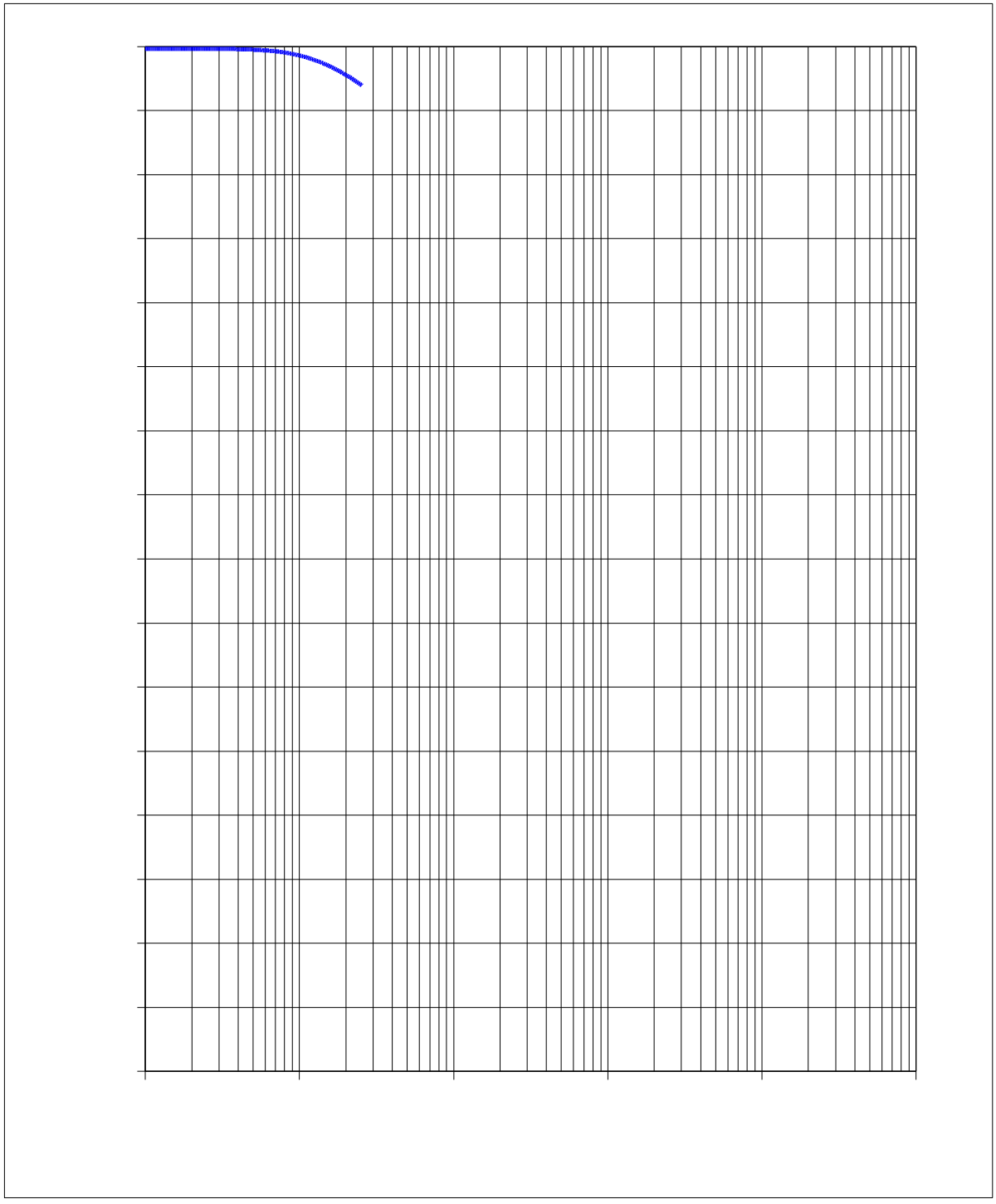

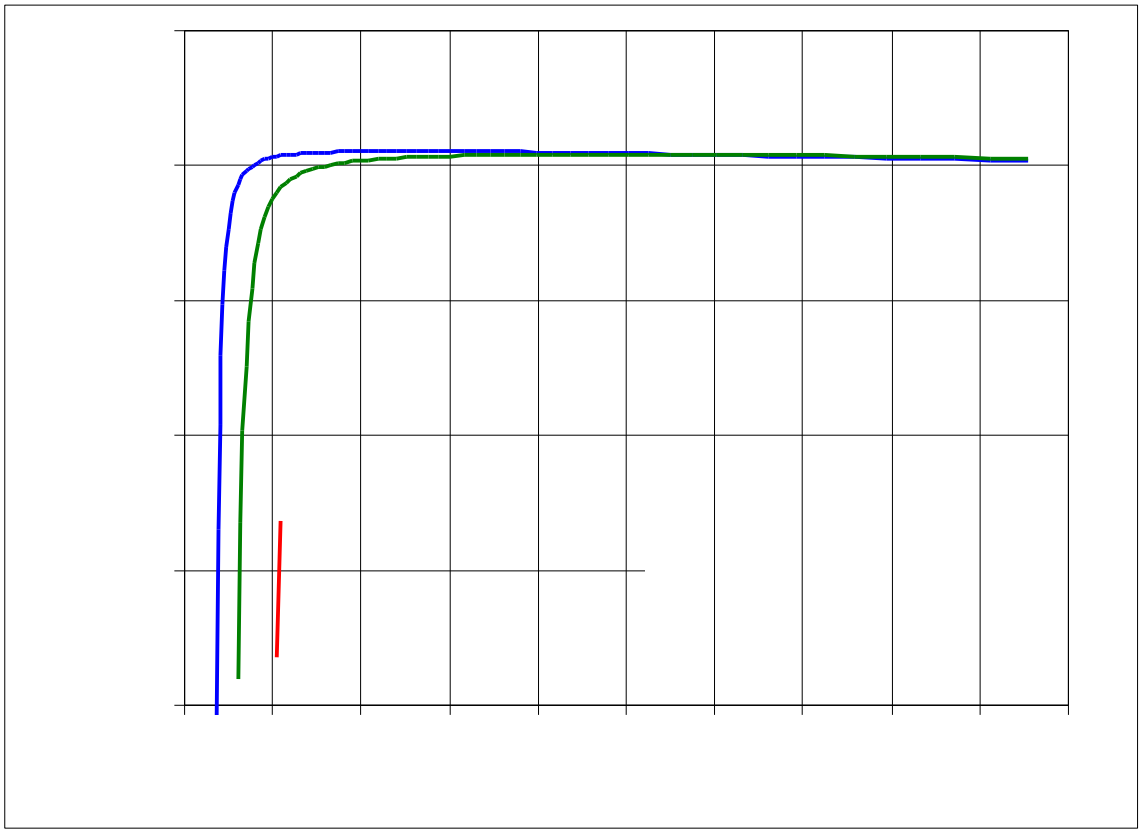

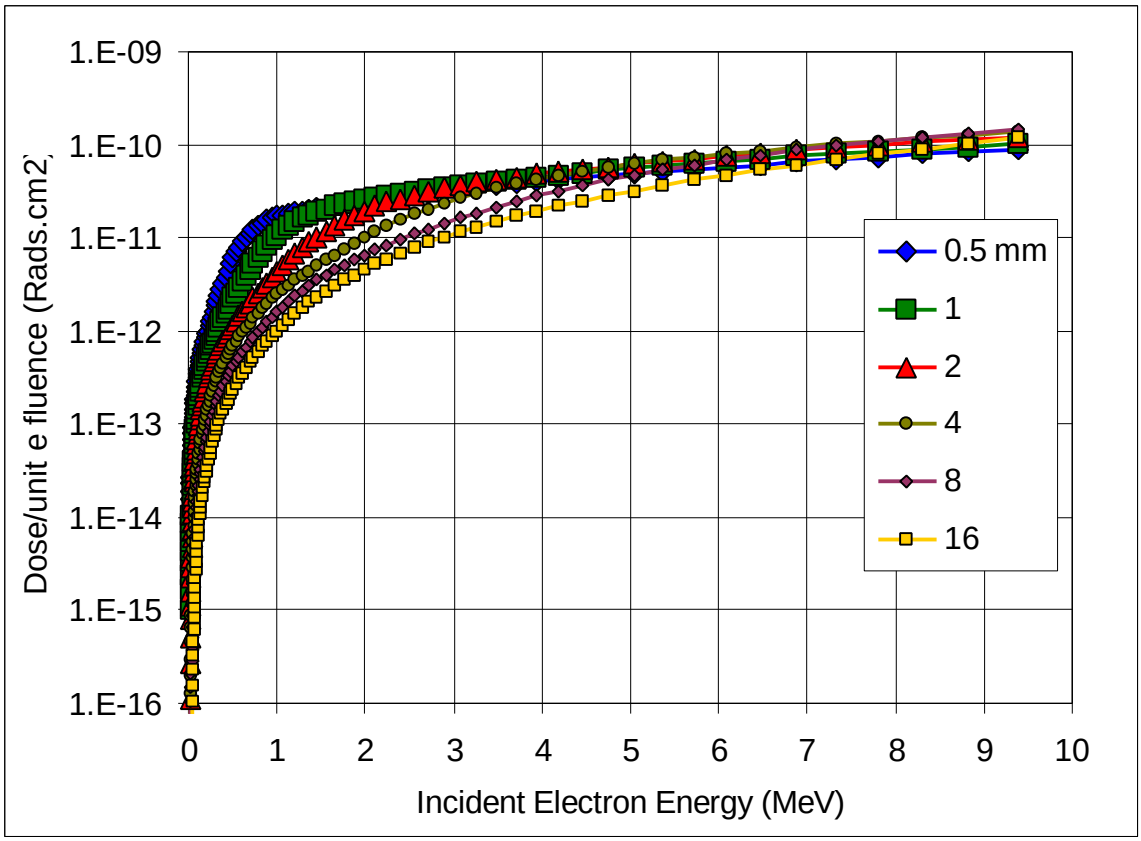

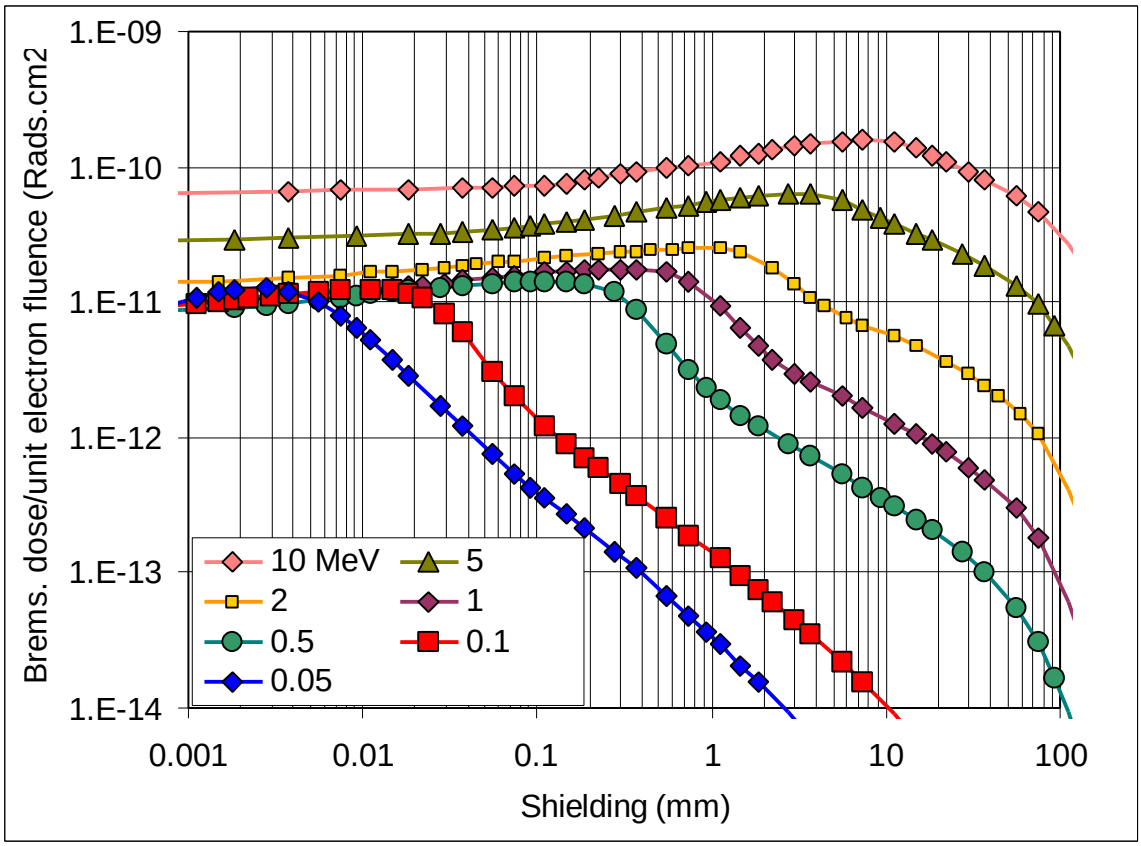

Figure 9-8 (continued): (b) Bremsstrahlung doses as a function of energy and depth

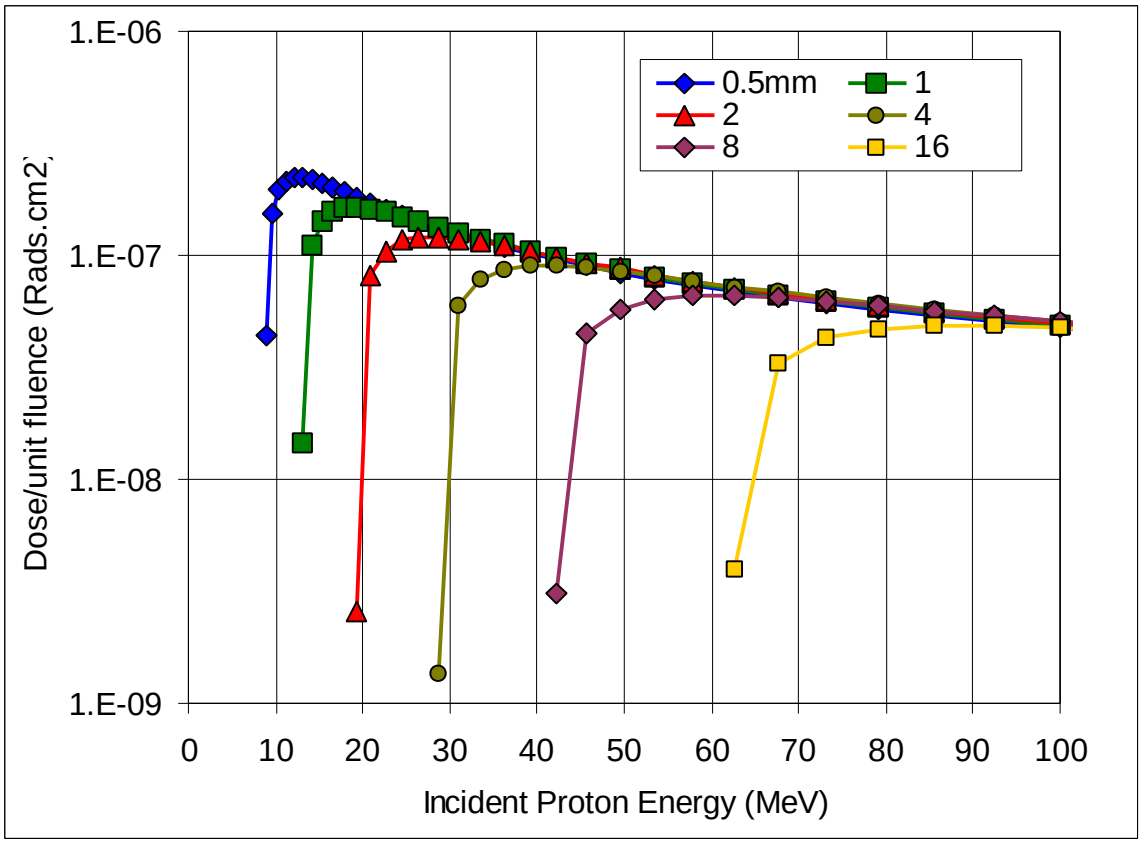
1.E-06
1.E-07
1.E-08
1.E-09
Dose/unit fluence (Rads.cm2)
0.5mm
1
2
4
8
16
0
10
20
30
40
50
60
70
80
90
100
Incident Proton Energy (MeV)

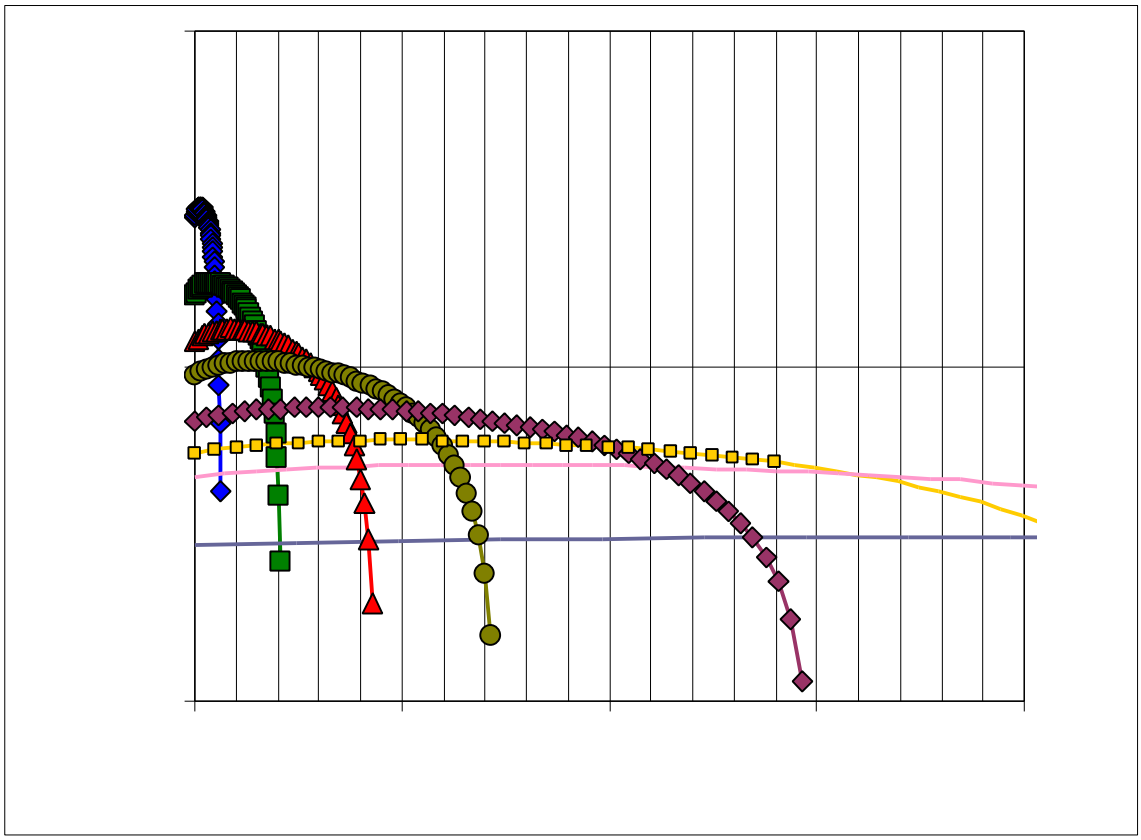

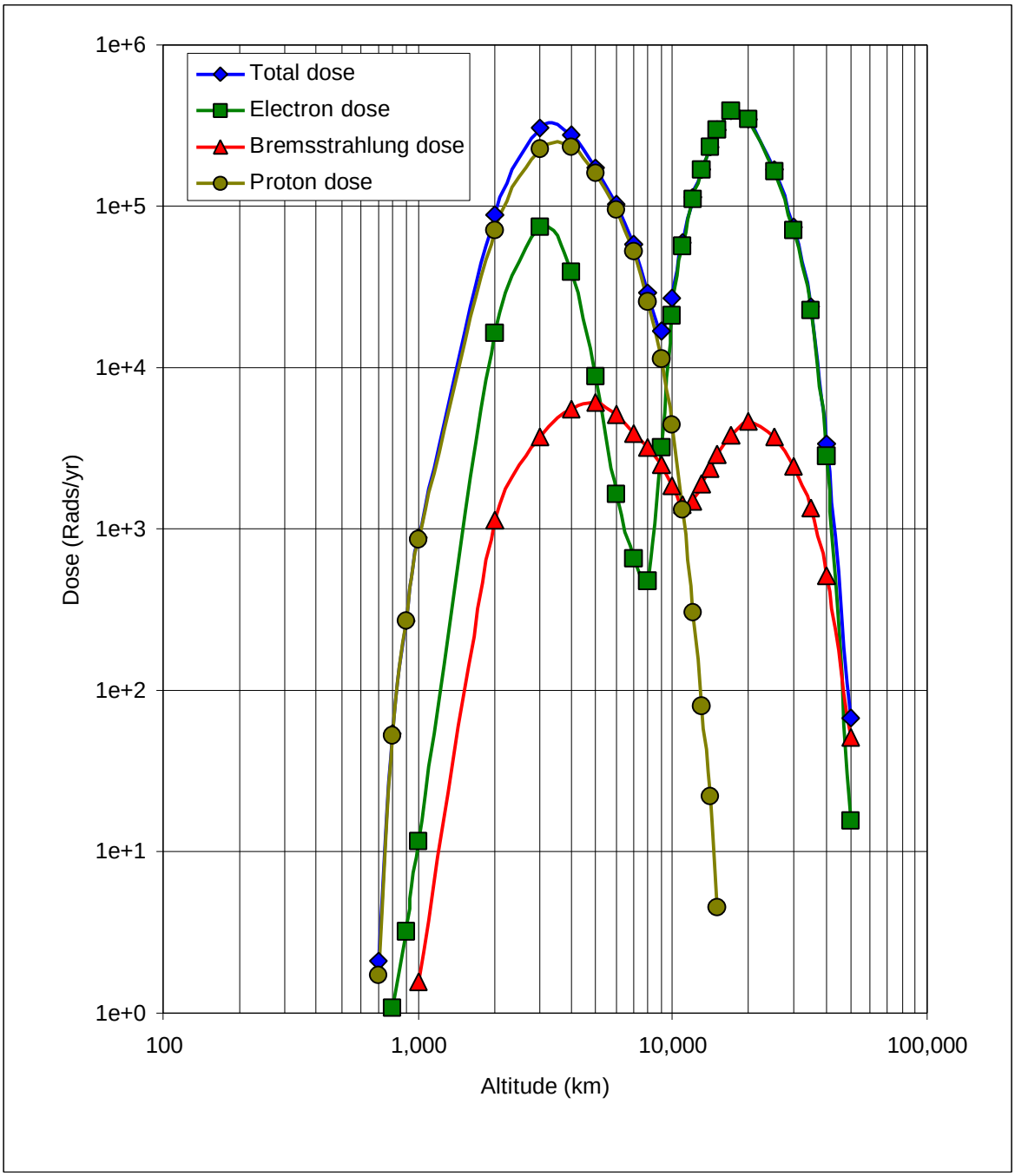

Figure 9-9 Annual doses behind 4mm spherical shielding on circular equatorial orbits in the radiation belts, as a function of orbit height.

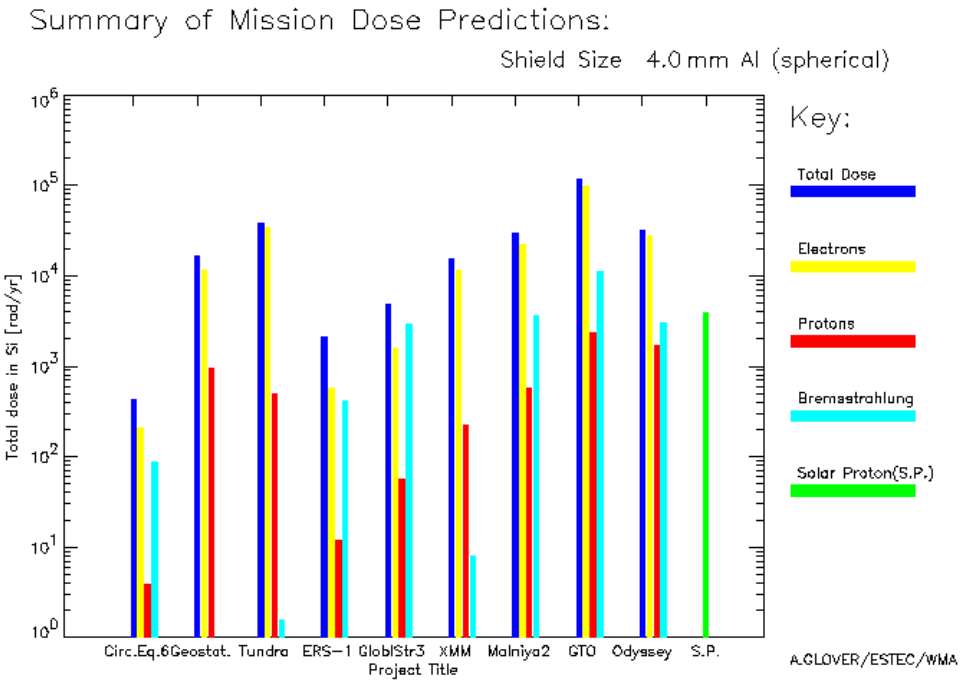

Figure 9-10 Typical doses predicted for typical missions

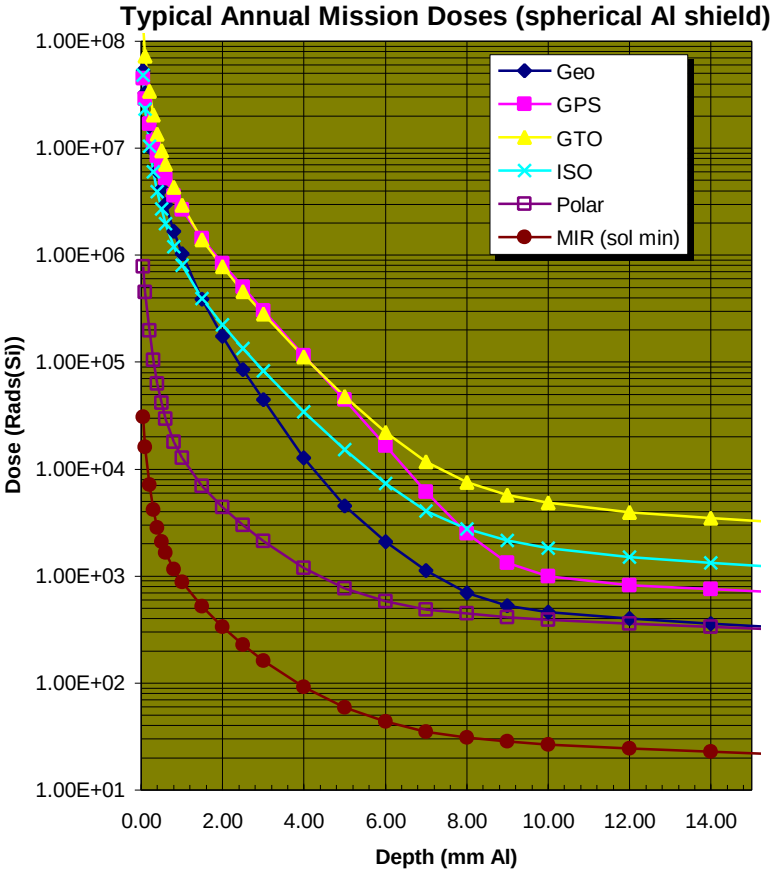

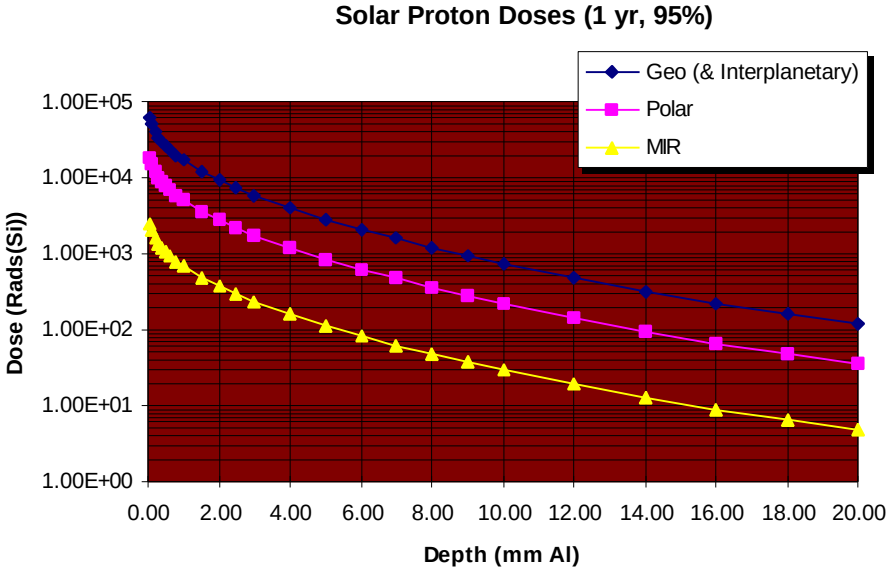

Figure 9-11 Typical Dose-Depth Curves for earth-orbits

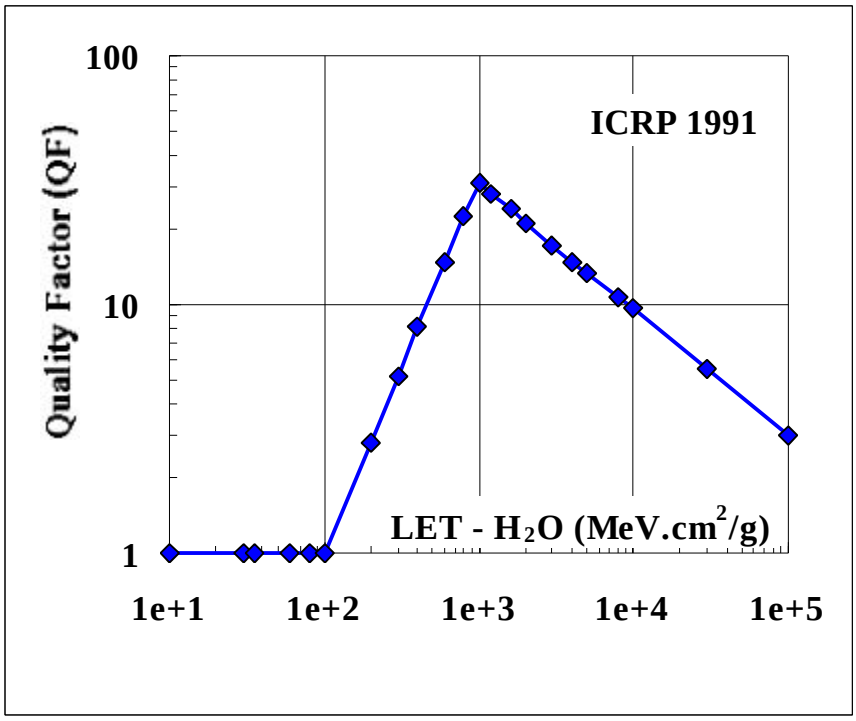

Figure 9-12 Quality factors for use in dose equivalent calculation for radio-biological effect purposes, as defined by the *ICRP*.

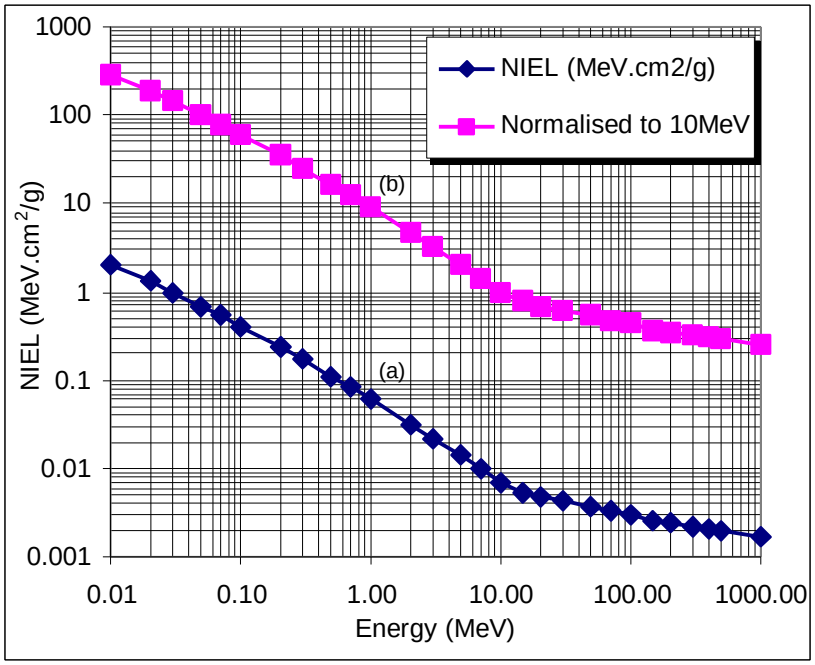

Figure 9-13 :NIEL curve: (a) energy lost by protons in non-ionizing interactions (bulk, displacement damage); (b) NIEL relative to 10MeV giving damage-equivalence of other energies.

9.9 References

RD9.1 Hess W.N., “The Radiation Belt and Magnetosphere”, Blaisdell Publ. Co.,1968

RD9.2 Daly, E.J., “The Radiation Belts”, Radiation Physics and Chemistry 43, 1, pp.1-18 (in Special Issue on Space Radiation Environment and Effects), 1994

RD9.3 NCRP, “Guidance on Radiation Received in Space Activities”, Report NCRP-98, National Council on Radiation Protection and Measurements, ISBN 0-929600-04-5, July 1989

RD9.4 ECSS, “Human Factors Standard”, ECSS-Q-TBD

RD9.5 ICRP, “1990 Recommendations of the International Commision on Radiological Protection”, ICRP Publication 60, Annals of the ICRP 21, 1-3 ISBN: 0-08-041144-4, Pergamon Press, NY and Oxford (1991)

RD9.6 Vette J.I. “The AE-8 Trapped Electron Model Environment”, NSSDC/WDC-A-R&S Report 91-24, NASA-GSFC (1991)

RD9.7 Sawyer D.M. and Vette J.I., "AP8 Trapped Proton Environment For Solar Maximum and Solar Minimum", NSSDC WDC-A-R&S 76-06, NASA-GSFC (1976).

RD9.8 Belian, R.D., T.E. Cayton, R.A. Christensen, J.C. Ingraham, M.M. Meier, G.D. Reeves and A.J. Lazarus, “Relativistic electrons in the outer-zone: An 11-year cycle; their relation to the solar wind”, Proceedings of the Taos Workshop on the Earth's Trapped Particle Environment, G.D. Reeves, ed., AIP Conference Proceedings 383, 13-18, ISBN 1-56396-540-2 (1986).

RD9.9 Watts J.W., Parnell T.A. and Heckman H.H., “Approximate Angular Distribution and Spectra for Geomagnetically Trapped Protons in Low-Earth Orbit", in High-Energy Radiation Background in Space, AIP Conference Proceedings 186, AIP, NewYork (1989).

RD9.10 Kruglanski M. and Lemaire J., “Trapped Proton Anisotropy at Low Altitude”, Technical Note 6, ESA/ESTEC/WMA Contr. 10725, BIRA(1996).

RD9.11 Bühler P., Zehnder A., Daly E. and Adams L., “REM Measurements on-Board MIR in 1995” Cospar General Assembly 1996, to appear in Adv. Sp. Res. 1997-1998.

RD9.12 Lemaire J., A.D. Johnstone, D. Heynderickx, D.J. Rodgers, S. Szita and V. Pierrard, “Trapped Radiation Environment Model Development (TREND-2)” Final Report of ESA Contr. 9828, Aeronomica Acta 393-1995, Institut d’Aeronomie Spatiale de Belgique / Belgisch Institut voor Rumte-Aeronomie,. ISSN 0065-3713. (1995).

RD9.13 Brautigam D.H., Gussenhoven M.S. and Mullen E.G., “Quasi-Static Model of Outer Zone Electrons”, IEEE Trans. Nucl. Sci. NS-39,.1797 (1992).

RD9.14 Singley G.W. and I. Vette J.I. "The AE-4 Model of the Outer Radiation Zone Electron Environment", NSSDC/WDC-A-R&S 72-06, NASA-GSFC (1972).

RD9.15 Tranquille C, “Extension to AE-4 Local Time and Statistical Models for Application to AE-8”, ESTEC/WMA Internal Memorandum, (1986).

RD9.16 Feynman J., Spitale G., Wang J. and Gabriel S., “Interplanetary Proton Fluence Model: JPL 1991”, J. Geophys. Res. 98, A8, 13281-13294 (1993).

RD9.17 Tranquille C. and E.J. Daly, "An Evaluation of Solar Proton Event Models for ESA Missions", ESA J. 16, 275 (1992).

RD9.18 King, J.H., “Solar Proton Fluences for 1977-1983 Space Missions”, J. Spacecraft & Rockets 11, 401, (1974)

RD9.19 Mathews J. and Towheed S., OMNIWeb, http://nssdc.gsfc.nasa.gov/omniweb/ mathews@nssdc.gsfc.nasa.gov, Code 633, NASA GSFC, Greenbelt, MD 20771, USA

RD9.20 National Geophysical Data Center, "Space Environment Data from NOAA's GOES Satellites", National Geophysical Data Center, Code E/GC2, Dept. 946 325 Broadway Boulder Co 80303 3328 USA., also Space Physics Interactive Data Resource at http://www.ngdc.noaa.gov:8080/

RD9.21 Adams, J.H., "Cosmic Ray Effects on MicroElectronics, Part IV", NRL Memorandum Report 5901, Naval Research Laboratory, Washington DC 20375-5000, USA (1986)

RD9.22 A.J. Tylka et al. "CREME96: A Revision of the Cosmic Ray Effects on Micro-Electronics Code", IEEE Trans. Nucl. Sci. NS-44, 2150-2160 (1997).

RD9.23 R.A. Nymmik, M.I. Panasyuk, T. I. Pervaja, and A.A. Suslov "A Model of Galactic Cosmic Ray Fluxes", by, Nucl. Tracks & Radiat. Meas, **20**, 427-429 (1992)

RD9.24 Adams J.H., Silberberg R. and Tsao C.H., "Cosmic Ray Effects on Microelectronics, Part I: The Near-Earth Particle Environment", NRL Memorandum Report 4506, Naval Research Laboratory, Washington DC 20375-5000, USA (1981).

RD9.25 Roberts C.S., `Coordinates for the Study of Particles Trapped in the Earth's Magnetic Field: A Method of Converting from *B,L* to *R,*λ Coordinates', J. Geophys. Res. 69, 5089, 1964.

RD9.26 Stassinopoulos E.G. and King J.H., "Empirical Solar Proton Model For Orbiting Spacecraft Applications", IEEE Trans. on Aerosp. and Elect. Systems AES-10, 442 (1973).

RD9.27 Seltzer S., 'SHIELDOSE: A Computer Code For Space Shielding Radiation Dose Calulations', NBS Technical Note 1116, National Bureau of Standards, May 1980 .

RD9.28 Petersen E.L., "Approaches to Proton Single-Event-Rate Calculation", IEEE Trans. Nucl. Sci. NS-43, 2 (special issue on Single Event Effects and the Space Environment), 496 (1996)

RD9.29 Pickel J.C., " Single-Event Effects Rate Prediction", IEEE Trans. Nucl. Sci. NS-43, 2 (special issue on Single Event Effects and the Space Environment), 483 (1996).

RD9.30 Tada H.Y., Carter J.R, Anspaugh B.E. & Downing R.G, " Solar Cell Radiation Handbook", 3rd Edition, JPL Publn. 82-69 (1982); Anspaugh B.E, "GaAs Solar Cell Radiation Handbook", JPL Publn. 96-9 (1996).

RD9.31